





Cite this: DOI: 10.1039/c7ee02477k

## Balancing gravimetric and volumetric hydrogen density in MOFs†

Alauddin Ahmed,<sup>a</sup> Yiyang Liu,<sup>b</sup> Justin Purewal,<sup>c</sup> Ly D. Tran,<sup>b</sup> Antek G. Wong-Foy,<sup>b</sup> Mike Veenstra,<sup>c</sup> Adam J. Matzger <sup>b</sup> and Donald J. Siegel <sup>\*adef</sup>

Metal organic frameworks (MOFs) are promising materials for the storage of hydrogen fuel due to their high surface areas, tunable properties, and reversible gas adsorption. Although several MOFs are known to exhibit high hydrogen densities on a gravimetric basis, realizing high volumetric capacities – a critical attribute for maximizing the driving range of fuel cell vehicles – remains a challenge. Here, MOFs that achieve high gravimetric and volumetric H<sub>2</sub> densities simultaneously are identified computationally, and demonstrated experimentally. The hydrogen capacities of 5309 MOFs drawn from databases of known compounds were predicted using empirical (Chahine rule) correlations and direct atomistic simulations. A critical assessment of correlations between these methods, and with experimental data, identified pseudo-Feynman–Hibbs-based grand canonical Monte Carlo calculations as the most accurate predictive method. Based on these predictions, promising MOF candidates were synthesized and evaluated with respect to their usable H<sub>2</sub> capacities. Several MOFs predicted to exhibit high capacities displayed low surface areas upon activation, highlighting the need to understand the factors that control stability. Consistent with the computational predictions, IRMOF-20 was experimentally demonstrated to exhibit an uncommon combination of high usable volumetric and gravimetric capacities. Importantly, the measured capacities exceed those of the benchmark compound MOF-5, the record-holder for combined volumetric/gravimetric performance. Our study illustrates the value of computational screening in pinpointing materials that optimize overall storage performance.

Received 30th August 2017,  
Accepted 11th October 2017

DOI: 10.1039/c7ee02477k

rsc.li/ees

### Broader context

The adoption of hydrogen fuel cell vehicles will benefit from the development of low-cost, high-capacity methods for storing hydrogen fuel. State-of-the-art storage systems are based on pressurized H<sub>2</sub> gas. These systems are bulky, expensive, and operate at high pressures up to 700 bar. Consequently, alternative storage strategies with the potential for higher efficiency and lower-cost are being explored. Of these, adsorptive storage in metal–organic frameworks (MOFs) presents one of the more promising approaches due to the moderate operating pressures, fast kinetics, reversibility, and high gravimetric densities typical of MOF-based storage. One area where MOFs struggle, however, is in achieving high volumetric H<sub>2</sub> densities. Ideally, a hydrogen adsorbent should exhibit high gravimetric and volumetric densities simultaneously. Unfortunately, achieving such a balance remains a challenge: for example, identifying MOFs that outperform the benchmark compound MOF-5 on a volumetric and gravimetric basis has proven difficult. The present study demonstrates IRMOF-20 as a MOF that surpasses MOF-5 on both a usable volumetric and gravimetric basis. Our approach demonstrates the power of high-throughput computational screening in guiding experimental synthesis & characterization efforts towards promising compounds. In so doing, a new high-water mark for volumetric hydrogen density in MOFs has been established.

<sup>a</sup> Mechanical Engineering Department, University of Michigan, Ann Arbor, MI 48109, USA. E-mail: djsiege@umich.edu; Tel: +1-734-764-4808

<sup>b</sup> Department of Chemistry, University of Michigan, Ann Arbor, MI 48109, USA

<sup>c</sup> Ford Motor Company, Research and Advanced Engineering, 1201 Village Rd., Dearborn, MI 48121, USA

<sup>d</sup> Materials Science & Engineering, University of Michigan, Ann Arbor, MI 48109, USA

<sup>e</sup> Applied Physics Program, University of Michigan, Ann Arbor, MI 48109, USA

<sup>f</sup> University of Michigan Energy Institute, University of Michigan, Ann Arbor, MI 48109, USA

† Electronic supplementary information (ESI) available: Detailed synthesis procedures, XRD patterns, N<sub>2</sub> isotherms, statistics, pore geometry, and tables of promising MOFs. See DOI: 10.1039/c7ee02477k

## Introduction

A high-capacity, low-cost method for storing hydrogen remains one of the primary barriers to the widespread commercialization of fuel cell vehicles (FCVs).<sup>1</sup> Although many storage technologies have been proposed, storage *via* adsorption presents one of the more promising approaches due to its fast kinetics, facile reversibility, and high gravimetric densities.<sup>1</sup>

Metal–organic frameworks (MOFs) are a relatively new class of adsorbents that have attracted intense interest as materials

for the capture and storage of gases.<sup>2–9</sup> MOFs are coordination compounds composed of metal clusters and organic linkers that form a crystalline network.<sup>10–17</sup> The surface area of MOFs can be extremely high, exceeding  $5000 \text{ m}^2 \text{ g}^{-1}$  in several compounds.<sup>11,12,18–26</sup> Moreover, the composition and structure of MOFs are highly tunable.<sup>27–30</sup>

Unfortunately, the design flexibility afforded by MOFs creates challenges for the identification of the best material for a given application. For example, many more MOFs exist than can be evaluated using conventional experimental techniques: several thousand MOFs have been synthesized, and  $\sim 10^5$  hypothetical compounds have been proposed.<sup>27–30</sup> An additional complexity is that the storage capacity of a MOF depends on several parameters, including: temperature, pressure, surface area, crystal density, pore volume, pore diameter,<sup>18</sup> pore size distribution,<sup>20,31</sup> heat of adsorption,<sup>32,33</sup> and others.<sup>34–37</sup>

To overcome these complications, several studies have turned to computational screening to accelerate the identification of high-performing MOFs.<sup>4,25,30,38,39</sup> In the case of hydrogen storage, Goldsmith *et al.*<sup>27</sup> created a database of computation-ready MOFs by mining the Cambridge Structural Database (CSD 2011).<sup>40</sup> More recently, Chung *et al.*<sup>28</sup> and Moghadam *et al.*<sup>29</sup> used variants of Goldsmith *et al.*'s method applied to later CSD versions, 2014 and 2017, respectively, to identify additional MOFs. Goldsmith *et al.*<sup>27</sup> used the empirical correlation between an adsorbent's surface area and its excess gravimetric uptake (the so-called Chahine rule)<sup>27,41</sup> to estimate the theoretical total hydrogen storage capacities of MOFs in their database. Several high-capacity MOFs were identified, many of which had not been assessed as  $\text{H}_2$  adsorbents. Examples included: DIDDOK,<sup>42</sup> EPOTAF (SNU-21),<sup>43</sup> and SUKYON.<sup>44</sup>

In addition to identifying promising MOFs, ref. 27 also uncovered a tradeoff between total volumetric and gravimetric  $\text{H}_2$  density. This tradeoff applies to compounds having large surface areas, and implies that MOFs with the highest gravimetric performance will generally exhibit modest volumetric capacities. This trend poses a new set of challenges, as prior analyses<sup>45–48</sup> have shown that the volumetric density of the hydrogen storage system more strongly impacts the driving range of a FCV than does the gravimetric density. Fig. 1 illustrates this effect.<sup>45–48</sup> For example, a storage system that falls 20% below the DOE 2025 gravimetric target<sup>46</sup> (corresponding to a few tens of kg increase in vehicle weight) is projected to reduce driving range by only  $\sim 1\%$ . In contrast, driving range is impacted significantly when the storage system fails to meet the volumetric target: a system that falls 20% below the DOE target results in a large,  $\sim 60 \text{ mi}$  decrease in driving range. Additional details regarding this analysis can be found in an earlier publication.<sup>47</sup>

Of course, an ideal hydrogen adsorbent should exhibit a balance of high volumetric and gravimetric  $\text{H}_2$  densities. Unfortunately, achieving high volumetric densities in MOFs remains a challenge, especially in comparison to the densities typical of metal hydrides.<sup>1</sup> Perhaps for this reason, reports of hydrogen storage in new MOFs have historically emphasized gravimetric performance.

The desire to balance gravimetric and volumetric performance led the Hydrogen Storage Engineering Center of Excellence

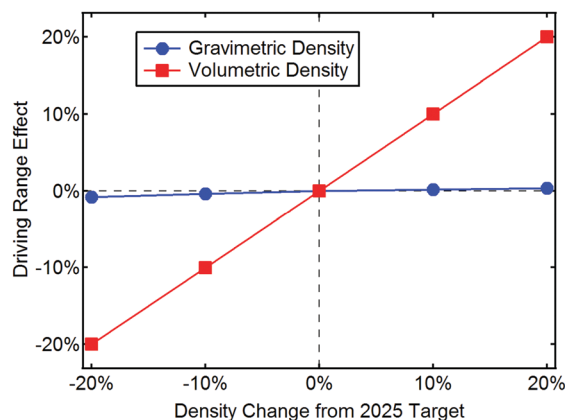


Fig. 1 Effect of  $\text{H}_2$  storage density on driving range. (blue curve) Percentage change in range as a function of gravimetric density, assuming the system achieves the 2025 volumetric target. (red curve) Percentage change in range as a function of volumetric density, assuming the system achieves the 2025 gravimetric target. Adapted from ref. 45–48.

(HSECoE) to select MOF-5 as the adsorbent medium for demonstration in two prototype hydrogen storage systems.<sup>45,48,49</sup> These prototyping studies have positioned MOF-5 as an important benchmark material, due to its unique balance of capacities, and despite its stature as one of the oldest, most widely-studied MOFs. Although more than 15 years of MOF research has occurred since its introduction, surpassing the performance of MOF-5 on a volumetric basis has been elusive.

The foregoing discussion raises several questions:

- (1) Can the compounds identified by Goldsmith *et al.* be synthesized and activated in a form that realizes their predicted (exceptional)  $\text{H}_2$  capacities?
- (2) How accurate is the Chahine rule as a predictive tool? Are direct atomistic simulations more reliable?
- (3) Can MOFs that balance usable gravimetric and volumetric  $\text{H}_2$  densities, and out-perform MOF-5, be demonstrated?

Regarding question 1 (MOF synthesis & activation): MOF synthesis can yield compounds with retained solvent molecules, defects, and disorder.<sup>27–29</sup> In contrast, computational models of MOFs are typically based on idealized crystal structures<sup>27,28</sup> where these flaws are absent. Consequently, the predictions derived from computational models represent best case scenarios that are not always realized in experiments. Reduction of guest-accessible surface area or pore volume upon activation, commonly known as “pore collapse,” is one explanation for this discrepancy. In summary, there is no guarantee that a given MOF can be experimentally realized in a ‘pristine’ form, even if that structure is present in a database of experimentally-derived crystal structures.

Regarding question 2 (validity of the Chahine rule): the Chahine rule – 1 wt% of excess adsorbed  $\text{H}_2$  is contributed for every  $500 \text{ m}^2 \text{ g}^{-1}$  of surface area – has been validated at 77 K and 35 bar for a handful of porous carbon materials and MOFs.<sup>50</sup> However, the limited availability of reproducible hydrogen storage measurements for a larger and more diverse set of MOFs presents a challenge to assessing the generality of the Chahine rule.<sup>51–54</sup>

H<sub>2</sub> storage capacities can also be predicted using grand canonical Monte Carlo<sup>55,56</sup> (GCMC) simulations.<sup>51,53,55</sup> The accuracy of GCMC depends on the accuracy of the MOF crystal structure and the interatomic potentials employed.<sup>51,53</sup> The Universal Force Field<sup>57</sup> (UFF) or one of its variants (e.g., UFF4MOF<sup>58,59</sup>) is typically adopted to describe the MOF atoms.<sup>51,53</sup> However, there is no consensus regarding an appropriate model for H<sub>2</sub> in the literature.<sup>51–54</sup> Many of the available H<sub>2</sub> models were initially validated using a small number of MOFs (sometimes using a single MOF), and subsequently adopted for large-scale simulations with limited additional scrutiny. Variability in experimental data<sup>50,54,60</sup> has also posed challenges for parameterization of accurate interatomic potentials. Overall, few H<sub>2</sub> models have been benchmarked against a diverse set of MOF isotherms and over a practical range of pressures.<sup>51,53</sup> Furthermore, as suggested by Feynman and Hibbs (FH), quantum mechanical effects can be important at the cryogenic temperatures typical of H<sub>2</sub> uptake measurements in MOFs ( $T = 77$  K).<sup>61,62</sup> For example, it has recently been reported that the use of the FH quantum correction with existing H<sub>2</sub> models reduces H<sub>2</sub> uptake predictions by 15 to 20% (compared to of the uncorrected values).<sup>52,63</sup> In summary, a combination of experimental and computational issues has slowed progress towards identifying a preferred method for predicting H<sub>2</sub> uptake in MOFs.

Regarding question 3 (new MOF discovery): recently, the HSECoE highlighted usable (rather than total) capacity as a performance metric for on-board H<sub>2</sub> storage.<sup>64</sup> Usable capacity is evaluated assuming a pressure swing between 5 bar (“empty vessel”) and 100 bar (“full vessel”). The pressure swing can be isothermal ( $T = 77$  K), or involve a temperature swing between 77 and 160 K.

As previously mentioned, a MOF-5-based adsorbent bed was used in sub-scale storage systems demonstrated by the HSECoE. To improve the performance of these systems it is desirable to identify alternative MOFs that surpass the usable capacity of MOF-5 (4.5 wt% & 31.1 g H<sub>2</sub> per L, pressure swing).<sup>50,65,66</sup> Unfortunately, predictions employing the Chahine rule are restricted to total capacities at a single pressure and temperature (35 bar and 77 K). It is therefore of limited value in predicting usable capacities. On the other hand, GCMC provides predictions of full isotherms, allowing for usable capacity estimates.

The goal of the present study is to answer questions 1 to 3 using a combination of computational screening, experimental synthesis, and H<sub>2</sub> uptake measurements. First, the performance of MOF-5 was carefully reassessed to provide an unambiguous baseline for comparison with other compounds. In addition to MOF-5, we evaluated the performance of three promising MOFs – DIDDOK, EPOTAF, and SUKYON – predicted<sup>27</sup> by the Chahine rule to out-perform MOF-5. However, after synthesis and activation the measured surface areas of these MOFs were observed to be significantly less than the theoretical predictions, likely due to pore collapse.

Subsequently, the total H<sub>2</sub> capacities of 5309 non-hypothetical MOFs compiled from the UM<sup>27</sup> and CoRE<sup>28</sup> databases were assessed using the Chahine rule and GCMC calculations.

A comparison of the GCMC and Chahine rule reveals a strong correlation in predicted capacities. Nevertheless, the Chahine rule generally over-predicts H<sub>2</sub> adsorption for MOFs with large surface areas ( $> \sim 4500$  m<sup>2</sup> g<sup>-1</sup>).

GCMC-based computational screening identified 90 compounds with usable capacities expected to surpass the MOF-5 baseline. Of these candidates, IRMOF-20 was identified as a candidate with potential to be synthesized and activated in a pristine form. Measurements on this compound demonstrated excellent agreement with the calculated surface area and H<sub>2</sub> isotherm. More importantly, IRMOF-20 demonstrated a usable H<sub>2</sub> capacity of 5.7 wt% and & 33.4 g H<sub>2</sub> per L at 77 K, assuming a pressure swing between 5 and 100 bar. This capacity surpasses that of MOF-5 on both a usable gravimetric and volumetric basis, thereby establishing a new benchmark for hydrogen storage in MOFs.

## Methodology

### MOF databases

We examined 5309 real (*i.e.*, non-hypothetical) MOFs from the UM<sup>27</sup> and CoRE<sup>28</sup> databases. Both of these databases were distilled from the Cambridge Structural Database (CSD)<sup>40</sup> using similar algorithms developed originally by Goldsmith *et al.*<sup>27</sup> The UM and CoRE MOF libraries are based on CSD releases from 2011 and 2014, respectively.

### Computational characterization of MOFs

The guest-accessible surface area (ASA), pore volume (PV), pore diameter (PD), pore aperture (PA), void fraction (VF), and pore size distribution were calculated using Zeo++.<sup>19,20,67</sup> (PA is defined as the smallest diameter encountered along the pore network, while the PD is the largest diameter of any internal cavity.) The atomic radii of the MOF atoms were assigned using default values in the Zeo++ library, which are in turn based on atomic radii suggested in the CSD.<sup>40</sup> Surface areas were calculated using a N<sub>2</sub> probe molecule with van der Waals diameter of 3.72 Å. Additionally, Brunauer–Emmett–Teller (BET) surface areas were calculated from N<sub>2</sub> isotherms predicted *via* grand canonical Monte Carlo<sup>55</sup> (GCMC) simulations. In this case the MOF atoms and N<sub>2</sub> molecules were modeled using Lennard-Jones interactions with parameters adopted from the Universal Force Field (UFF)<sup>57</sup> and from the Transferable Potentials for Phase Equilibria (TraPPE),<sup>68</sup> respectively. Lorentz–Berthelot<sup>69,70</sup> combination rules were used in computing MOF-N<sub>2</sub> cross-interaction parameters. Finally, helium void fractions<sup>71</sup> of all synthesized MOFs were calculated using the method of Talu and Myer<sup>71</sup> employing the RASPA<sup>72,73</sup> package.

### Semi-empirical prediction of total hydrogen capacities

The total gravimetric and volumetric hydrogen capacities of all MOFs were evaluated at 77 K and 35 bar using the Chahine rule<sup>41,74</sup> and the procedure described in Goldsmith *et al.*<sup>27</sup> The Chahine rule is an empirical correlation stating that the excess gravimetric adsorption of hydrogen ( $n_{\text{ex}}$ ) is directly proportional

to the N<sub>2</sub>-accessible BET surface area (SA<sub>grav</sub>), *i.e.*,  $n_{\text{ex}} = C \times \text{SA}_{\text{grav}}$ . Here,  $C$  is a proportionality constant equal to  $2.1 \times 10^{-5}$  g H<sub>2</sub> per m<sup>2</sup> at 77 K and 35 bar. The total storage capacity ( $n_{\text{tot}}$ ) can be estimated by adding a contribution that accounts for gas phase H<sub>2</sub> ( $n_{\text{gas}}$ ) in the MOF pores:<sup>27</sup>

$$n_{\text{tot}} = n_{\text{ex}} + n_{\text{gas}} = C \cdot \text{SA}_{\text{grav}} + \rho_{\text{H}_2} V_{\text{pore}}, \quad (1)$$

where  $V_{\text{pore}}$  is the pore volume (in cm<sup>3</sup> g<sup>-1</sup>) and  $\rho_{\text{H}_2}$  is the density of hydrogen (0.0115 g cm<sup>-3</sup>) at 77 K and 35 bar. The total gravimetric (in wt%) and volumetric (g H<sub>2</sub> per L MOF) capacities can be obtained, respectively, by dividing  $n_{\text{tot}}$  by the summed mass of the MOF and H<sub>2</sub> stored, or by the volume of the unit cell.<sup>27</sup>

### Interatomic potentials

Hydrogen molecules were modeled using the pseudo-Feynman-Hibbs-corrected (p-FH) united-atom model proposed by Fisher *et al.*<sup>75</sup> The use of a (spherical) united atom model is reasonable, given that H<sub>2</sub> retains its rotational degrees of freedom even after adsorption<sup>62</sup> at cryogenic temperatures. The p-FH model was developed by adjusting the Lennard-Jones parameters to reproduce the Feynman-Hibbs-corrected Buch<sup>76</sup> potential at 77 K. Fisher *et al.*<sup>75</sup> verified that the p-FH model reproduced measured H<sub>2</sub> densities at 77 K and at various pressures. The model has also been shown to predict H<sub>2</sub> isotherms in good agreement with experimental measurements on MOF-5, MOF-74, ZIF-8, HKUST-1, MOF-505, UCMC-150, and (Mn<sub>4</sub>Cl)<sub>3</sub> (1,3,5-benzenetristetrazolate)<sub>8</sub> over a pressure range of 1 to 100 bar.<sup>75</sup> The p-FH model was selected based on a comparison of 5 popular H<sub>2</sub> models for their accuracy in reproducing H<sub>2</sub> isotherms measured in-house: p-FH, Kumar,<sup>77</sup> Buch,<sup>76</sup> Darkrim-Levesque,<sup>78,79</sup> and MGS.<sup>80,81</sup>

MOFs were modeled as a rigid framework using Lennard-Jones parameters from the UFF.<sup>57</sup> Interactions between MOF atoms and H<sub>2</sub> molecules were computed using Lorentz-Berthelot<sup>69,70</sup> combination rules. All H<sub>2</sub>-MOF interactions were truncated at 12 Å. MOFs with unit cell dimensions smaller than twice the cutoff radius were modeled with computational cells that were replicated periodically in the short direction(s). The crystalline nature of MOFs was accounted for by using periodic boundary conditions in all simulations.

### Grand canonical Monte Carlo simulation

Hydrogen storage capacities were computed using GCMC<sup>55,56,73,82,83</sup> simulations using the RASPA<sup>72</sup> package. Most simulations were performed using isothermal conditions with  $T = 77$  K over a

pressure range between 1 and 100 bar. Isotherms depicting the total stored H<sub>2</sub> were evaluated at several pressures within this pressure window. H<sub>2</sub> capacity was determined at each pressure on the isotherm by averaging the number of H<sub>2</sub> molecules in the simulation cell over 10 000 GCMC production cycles, preceded by 10 000 initialization cycles.<sup>39</sup> Each GCMC cycle was comprised of moves equal to the number of molecules in the system at the beginning of the cycle. Translation, insertion, and deletion moves were performed with equal probabilities.

### Selection of MOFs for synthesis

MOF-5 was selected as a benchmark compound due to its rare balance of gravimetric and volumetric H<sub>2</sub> capacities.<sup>27,84</sup> Despite the prominence of MOF-5 – it is by far the most widely-studied MOF – consensus regarding its hydrogen capacity has been slow to emerge; literature reports of its H<sub>2</sub> uptake exhibit a wide range of capacities.<sup>54</sup>

MOF-5 was synthesized following the procedure of ref. 65 as closely as possible. Subsequently, its surface area and H<sub>2</sub> isotherms were measured after careful activation. These data were compared to computational predictions, literature reports, and to values obtained for the pre-commercial version of MOF-5 used by the HSECoE.<sup>84</sup>

In addition to MOF-5, three MOFs with CSD identifiers SUKYON, DIDDOK, and EPOTAF (SNU-21) were selected for synthesis based on the Chahine rule predictions of Goldsmith *et al.*<sup>27</sup> that these compounds should exhibit high total capacities, exceeding that of MOF-5. Finally, IRMOF-20 was selected for synthesis based on GCMC screening performed in the present study. The crystal structures for these MOFs are shown in Fig. 2.

### MOF synthesis and characterization

All MOFs were synthesized using the methods reported earlier; additional details are provided in the ESI.† MOF-5 and IRMOF-20 were activated by solvent exchange with dichloromethane and drying under vacuum. Flowing supercritical CO<sub>2</sub> was used to activate SUKYON, EPOTAF (SNU-21), and DIDDOK. This method has been previously shown to be effective in realizing high surface areas in MOFs that tend to undergo pore collapse during activation,<sup>85,86</sup> and in MOFs where it is difficult to remove solvent of synthesis<sup>85,86</sup> with conventional activation techniques.<sup>87</sup>

Materials were characterized by powder X-ray diffraction (PXRD), using a Bruker D8 Advance diffractometer equipped

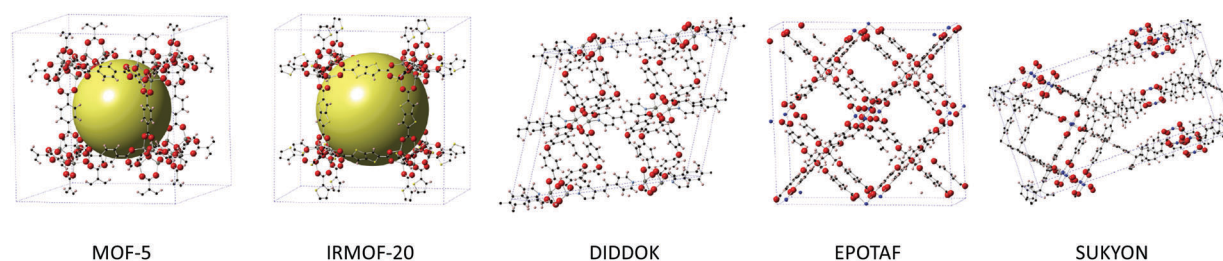


Fig. 2 Crystal structures of MOFs examined experimentally in this study.



with a 60 mm sealed Göbel mirror and a LynxEye linear position sensitive detector. The Cu-K $\alpha$  (1.5406 Å) X-ray source was operated at 40 kV and 40 mA. Samples were deposited on glass slides for measurement. Alternatively, a Rigaku R-Axis SPIDER diffractometer with an imaging plate detector using graphite monochromated Cu-K $\alpha$  radiation (1.5406 Å) operating at 40 kV and 44 mA was used. For collections at room temperature, samples were mounted on a cryoloop. To obtain powder patterns with minimized preferred orientation, images were collected for 3–5 minutes while rotating the sample about the  $\phi$ -axis at  $10^\circ \text{ s}^{-1}$  while oscillating  $\omega$  between  $120^\circ$  and  $180^\circ$  at  $1^\circ \text{ s}^{-1}$  and  $\chi$  set at  $45^\circ$ . Images were integrated in the AreaMax2 software package. The BET surface areas were measured by nitrogen adsorption and desorption at 77 K from 0.005 to 1 bar using a NOVA e-series 4200 surface area analyzer from Quantachrome Instruments (Boynton Beach, Florida, USA). Confirmatory measurements of BET surface areas were performed on a Micromeritics ASAP 2420 surface area analyzer. Surface areas were calculated from measured  $\text{N}_2$  isotherms following the recommendations by Roquerol<sup>88</sup> for the application of the BET method to microporous adsorbents.

Hydrogen adsorption and desorption measurements were performed using a manometric Sievert's-type instrument (HPVA-200, Micromeritics Instrument Corporation). Void volume measurements were performed using helium at room temperature to estimate both the internal volume of an empty sample cell, and the skeletal density ( $\rho_{\text{sk}}$ ) of the microporous sample ( $\rho_{\text{sk}} = 2.41 \text{ g cm}^{-3}$  was measured for IRMOF-20, and  $\rho_{\text{sk}} = 2.01 \text{ g cm}^{-3}$  for MOF-5). The mass of sample loaded for hydrogen adsorption measurements was 226 mg for MOF-5 and 563 mg for IRMOF-20. Samples were not heated prior to measurements since no significant residual water or solvent was detected on the vacuum gauge at room temperature. Hydrogen adsorption measurements were performed at 77 K, with the sample cell immersed in a liquid  $\text{N}_2$  bath. The ambient volume (sub-volume at room temperature) and cold volume (sub-volume at 77 K) of an empty sample cell was calibrated with the liquid  $\text{N}_2$  bath filled to a marked level on the sample cell stem. For subsequent 77 K measurements on IRMOF-20 and MOF-5, the free volume was calculated by subtracting the skeletal volume of the adsorbent (*i.e.*,  $= m/\rho_{\text{sk}}$ ) from the empty sample cell volume. Excess adsorption and desorption isotherms were measured using the static manometric method.<sup>88</sup>

Total hydrogen volumetric and gravimetric storage capacities were calculated following the recommendations made by Parrilla *et al.*,<sup>89</sup> using the MOF single crystal density ( $\rho_{\text{crys}} = 0.51 \text{ g cm}^{-3}$  for IRMOF-20, and  $\rho_{\text{crys}} = 0.61 \text{ g cm}^{-3}$  for MOF-5) in place of a packing density. Volumetric capacity in units of  $\text{g H}_2$  per L was calculated as

$$n_v = \rho_{\text{crys}} n_{\text{ex}} + \rho_{\text{gas}} \left( 1 - \frac{\rho_{\text{crys}}}{\rho_{\text{sk}}} \right), \quad (2)$$

where  $n_{\text{ex}}$  is the excess adsorption in units of  $\text{g kg}^{-1}$ , the crystal and skeletal densities have units of  $\text{g cm}^{-3}$ , and the bulk  $\text{H}_2$

density ( $\rho_{\text{gas}}$ ) has units  $\text{g L}^{-1}$ . Total gravimetric uptake (in wt%) is calculated from the volumetric uptake, as:

$$n_g = \frac{n_v}{n_v + 1000 \cdot \rho_{\text{crys}}} \times 100 \quad (3)$$

## Results and discussion

### Evaluation of MOF-5

MOF-5 crystals were observed to form during synthesis at  $80^\circ \text{C}$  after 32 h. The crystals were clear colorless cubes (as expected), while the solvent, diethylformamide, took on a yellow color. At this point heating was stopped, and the mixture was allowed to cool to room temperature. The yield of MOF-5 was less than 15%. Although continued heating could produce a higher yield, once the solvent darkens the crystallites exhibit a yellow hue that cannot be removed by washing with fresh solvent. Subsequently, all manipulations were carried out under inert atmosphere and with anhydrous solvents.

The predicted ( $3563 \text{ m}^2 \text{ g}^{-1}$ ) and measured ( $3512 \text{ m}^2 \text{ g}^{-1}$ , see Fig. S1, ESI† for the  $\text{N}_2$  isotherm)  $\text{N}_2$ -accessible BET surface areas of the in-house synthesized version of MOF-5 are in excellent agreement, and very similar to the theoretical value predicted by Gómez-Gualdrón *et al.*<sup>18</sup> ( $3434 \text{ m}^2 \text{ g}^{-1}$ ) and the measured BET surface area of the pre-commercial MOF-5 ( $3539 \text{ m}^2 \text{ g}^{-1}$ ) used by the HSECoE.<sup>84</sup> The measured surface area of our MOF-5 is larger than those reported by Panella *et al.*<sup>41</sup> ( $2296 \text{ m}^2 \text{ g}^{-1}$ ), Poirier and Dailly<sup>90</sup> ( $3100 \text{ m}^2 \text{ g}^{-1}$ ), and Durette *et al.*<sup>54</sup> ( $3201 \text{ m}^2 \text{ g}^{-1}$ ), but approximately  $300 \text{ m}^2 \text{ g}^{-1}$  smaller than that reported by Kaye *et al.*<sup>65</sup> ( $3800 \text{ m}^2 \text{ g}^{-1}$ ). Furthermore, our measured and calculated values are both similar to a recently reported<sup>18</sup> BET surface area of MOF-5 ( $3492 \text{ m}^2 \text{ g}^{-1}$ ) obtained through careful application of the Rouquerol *et al.*<sup>91,92</sup> criteria to an  $\text{N}_2$  isotherm obtained from GCMC calculations. Gómez-Gualdrón *et al.*<sup>18</sup> discussed how overlap of pore-filling and monolayer formation can lead to disagreement in calculated and measured surface areas. However, the calculated pore and aperture diameters of MOF-5 (see Fig. S2 and Table S1, ESI†) suggest that pore-filling contamination is not an issue for this MOF.

The PXRD pattern of our synthesized MOF-5 was compared with that obtained for pre-commercial MOF-5 provided by the HSECoE (Fig. S3 and S4, ESI†);<sup>84</sup> a very good match was obtained. Fig. 3 shows the measured hydrogen isotherms for the synthesized version of MOF-5, and for the MOF-5 provided by the HSECoE.<sup>84</sup> Consistent with their nearly-identical surface areas, the hydrogen isotherms from these two samples are almost indistinguishable. The isotherm reported by Kaye *et al.*<sup>65</sup> is also shown for comparison, and exhibits a higher  $\text{H}_2$  uptake.

### Synthesis and evaluation of MOFs predicted by Goldsmith *et al.*

A comparison of measured and simulated (generated using crystal structures) PXRD patterns was used to assess success at synthesizing, in guest free form, three of the promising MOFs predicted by Goldsmith *et al.*<sup>27</sup> DIDDOK, EPOTAF and SUKYON. All three patterns, upon solvent removal, showed that structural

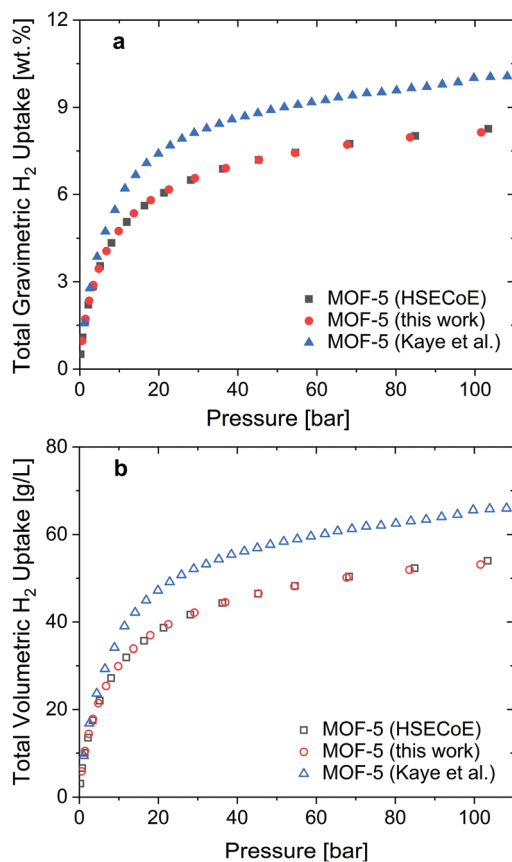


Fig. 3 Comparison of total (a) gravimetric and (b) volumetric  $\text{H}_2$  isotherms at 77 K for MOF-5 (this work), MOF-5 provided by the HSECoE, and MOF-5 reported by Kaye *et al.*<sup>65</sup>

integrity was not maintained. The PXRD pattern for DIDDOK is shown in Fig. S5 (ESI<sup>†</sup>) after activation. Differences in the patterns are dramatic and consistent with a substantial change in structure such that the crystal structure is no longer representative of the material. Similar behavior was observed for SUKYON (Fig. S6, ESI<sup>†</sup>) and EPOTAF (Fig. S7, ESI<sup>†</sup>).

Table 1 summarizes the measured and calculated crystallographic properties of SUKYON, EPOTAF, and DIDDOK. (Fig. S8–S10, ESI<sup>†</sup> show the  $\text{N}_2$  isotherms used in surface area measurements.) The measured BET surface area of SUKYON following activation by flowing supercritical  $\text{CO}_2$  (sc- $\text{CO}_2$ ) was  $2125 \text{ m}^2 \text{ g}^{-1}$ . This value is less than half the calculated geometric surface area,  $4577 \text{ m}^2 \text{ g}^{-1}$ .<sup>27</sup> The low measured surface area is consistent with Ma *et al.*'s<sup>44</sup>

Table 1 Measured and calculated properties of MOFs examined in this study. Values with an asterisk were reported in Goldsmith *et al.*<sup>27</sup>

MOF	Surface area	Pore vol.	Pore	Void
	( $\text{m}^2 \text{ g}^{-1}$ )	( $\text{cm}^3 \text{ g}^{-1}$ )	diameter ( $\text{\AA}$ )	
	Expt./calc.	Calc.	Calc.	Calc.
MOF-5	3512/3563	1.36	15.1	0.81
SUKYON	2125/4577*	1.47	10.8	0.77
EPOTAF	27/5208*	1.34	7.6	0.77
DIDDOK	578/4651*	1.48	9.6	0.78
IRMOF-20	4073/4127	1.65	17.3	0.84

reported BET values of  $526 \text{ m}^2 \text{ g}^{-1}$  and  $1560 \text{ m}^2 \text{ g}^{-1}$  upon vacuum- and freeze-drying (FD) activation, respectively. Ma *et al.*<sup>44</sup> attributed the discrepancy between the measured and calculated surface areas to a structural phase change during FD activation.

The measured BET surface area of EPOTAF after sc- $\text{CO}_2$  activation was only  $27 \text{ m}^2 \text{ g}^{-1}$ , which is over two orders of magnitude smaller than the calculated surface area of  $5208 \text{ m}^2 \text{ g}^{-1}$ .<sup>27</sup> Similar behavior was observed for DIDDOK, where the measured BET surface area after sc- $\text{CO}_2$  activation was only  $578 \text{ m}^2 \text{ g}^{-1}$ , while the predicted surface area is  $4651 \text{ m}^2 \text{ g}^{-1}$ .<sup>27</sup>

The large differences in the calculated and measured surface areas, along with similar differences in the measured diffraction patterns (compared to those based on single crystal structures), suggest that these three MOFs undergo pore collapse (or some other form of porosity-decreasing structure change<sup>85,86,93</sup>) during, or after, activation. In particular, the extremely low surface areas of EPOTAF and DIDDOK may be explained by their use of flexible linkers,<sup>94</sup> which greatly increases the likelihood of pore collapse in these compounds. A detailed comparison of pore geometries of all MOFs studied here can be found in Section 3 of the ESI.<sup>†</sup>

In summary, several of the promising MOFs predicted by Goldsmith *et al.*<sup>27</sup> to have high hydrogen capacities could not be realized experimentally. We emphasize that these compounds are MOFs previously reported in the literature, whose structures were extracted from the CSD. Their properties (surface area,  $\text{H}_2$  uptake) were predicted using algorithms known to correlate strongly with measured values. Nevertheless, the robustness of a given MOF against pore collapse remains a challenging property to predict. More effort is needed to address this failure mode, especially in MOFs predicted to have exceptionally-high surface areas. Below, we broaden our search for MOFs that can out-perform MOF-5, and successfully demonstrate IRMOF-20 as one such compound.

### Validation of interatomic potentials

In our prior work the semi-empirical Chahine rule was used to identify MOFs with high  $\text{H}_2$  capacities. The present study extends that approach using atomistic simulations based on grand canonical Monte Carlo (GCMC).<sup>55,95</sup> GCMC simulations are widely used to study gas uptake in porous materials.<sup>4,38</sup> An important advantage of GCMC is that it can predict uptake at arbitrary pressures and temperatures. This allows for simulation of full isotherms, and estimates of usable capacities, with the latter quantities measured as differences between two  $P, T$  state points.

For a GCMC calculation to be useful it must make accurate predictions of  $\text{H}_2$  uptake. This accuracy is largely determined by the details of the interatomic potential. To maximize the accuracy of our GCMC calculations, 5 popular potential models for hydrogen were assessed against hydrogen adsorption measurements involving MOF-5.

Fig. 4 compares the measured and simulated total hydrogen isotherms for MOF-5 at 77 K for pressures ranging from 1 to 100 bar. (The measured capacities of MOF-5 are provided in Table S2, ESI.<sup>†</sup>)

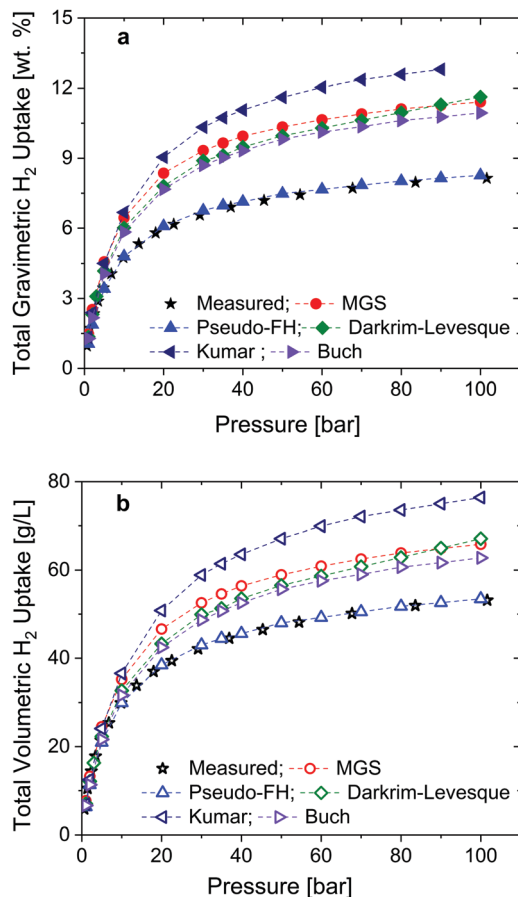


Fig. 4 Comparison of H<sub>2</sub> isotherms calculated with 5 different hydrogen models with measured total (a) gravimetric and (b) volumetric isotherms of MOF-5 at 77 K.

These data show that four of the five potentials – all except the p-FH – significantly over-predict H<sub>2</sub> uptake. The error is largest for the Kumar<sup>77</sup> potential, whose prediction for volumetric capacity is 41% higher than the measured value at 100 bar. Smaller, but still significant over-estimates are observed for the MGS<sup>80,81</sup> (20% higher) and Darkrim–Levesque<sup>78,79</sup> (16% higher) models, which are two of the most widely-used potentials. The performance of the Buch potential is similar to the Darkrim–Levesque model. In contrast, the isotherms predicted with the p-FH<sup>75</sup> model are in very good agreement with the measurements. Earlier studies have also shown that the bulk properties of hydrogen at 77 K are accurately reproduced by the p-FH potential.<sup>96,97</sup>

Comparisons with several other MOFs were performed to confirm the promising performance of the p-FH model. Fig. 5 illustrates these comparisons with in-house synthesized versions of MOF-5, UCMC-4,<sup>98</sup> MOF-177, MOF-177-NH<sub>2</sub>,<sup>99</sup> and DUT-23(Co),<sup>100</sup> data for the MGS potential is also shown for MOF-5 and UCMC-4. In all cases the isotherms generated from the p-FH model are in very good agreement with uptake measurements. Based on its ability to reproduce experimental isotherms, the p-FH model was adopted for subsequent screening studies.

Table 2 compares the measured and p-FH GCMC calculated usable H<sub>2</sub> storage capacities of MOF-5 at 77 K, assuming a pressure

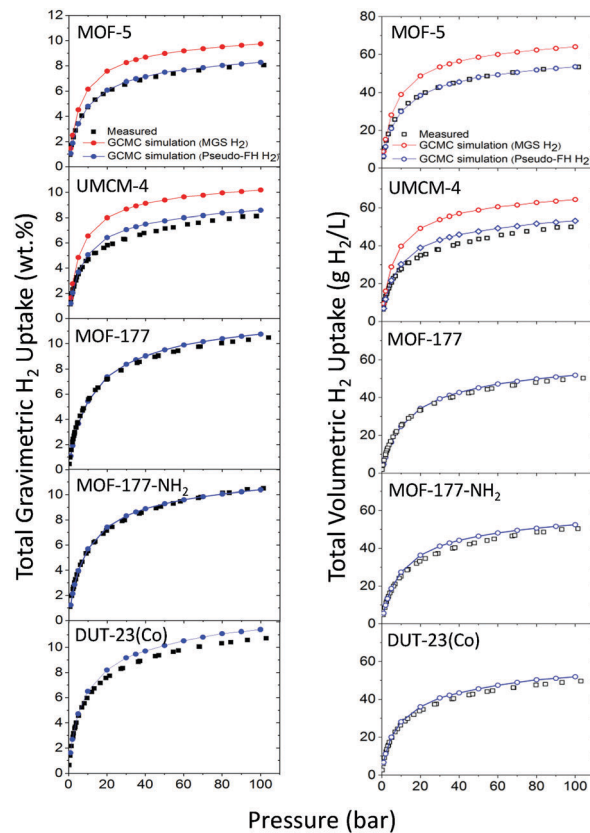


Fig. 5 Comparison of measured H<sub>2</sub> isotherms for several MOFs with those calculated with GCMC using the p-FH potentials. (left) Total gravimetric capacity; (right) total volumetric capacity. Additional comparisons are made to the MGS potential in the case of MOF-5 and UCMC-4.

Table 2 Comparison of calculated and measured usable H<sub>2</sub> capacities of in-house synthesized MOF-5 at 77 K assuming an isothermal pressure swing between  $P_{\min} = 5$  bar and  $P_{\max}$ . MUE is the mean unsigned error between the measurements and calculations

$P_{\max}$ (bar)	Usable gravimetric (wt%)		Usable volumetric (g H <sub>2</sub> per L)	
	Expt.	GCMC	Expt.	GCMC
35	3.3	3.6	22.2	23.5
50	3.8	4.1	25.6	27.0
100	4.5	4.9	31.1	32.5
MUE		0.3		1.4

swing between  $P_{\min} = 5$  bar and  $P_{\max} = 35, 50,$  and 100 bar (see Table S2, ESI† for the total H<sub>2</sub> capacities at these pressures). Good agreement between measurements and simulations is obtained, as is evident from the mean unsigned error (MUE): 0.3 wt% (gravimetric) and 1.4 g L<sup>-1</sup> (volumetric). (MUE is defined as the arithmetic mean of the absolute difference between the measured and calculated usable uptake across the different  $P_{\max}$  values.)

### Chahine rule vs. GCMC

We next quantify the extent to which H<sub>2</sub> capacity predictions made by the Chahine rule correlate with those derived from GCMC calculations. Fig. 6 illustrates these correlations for a set

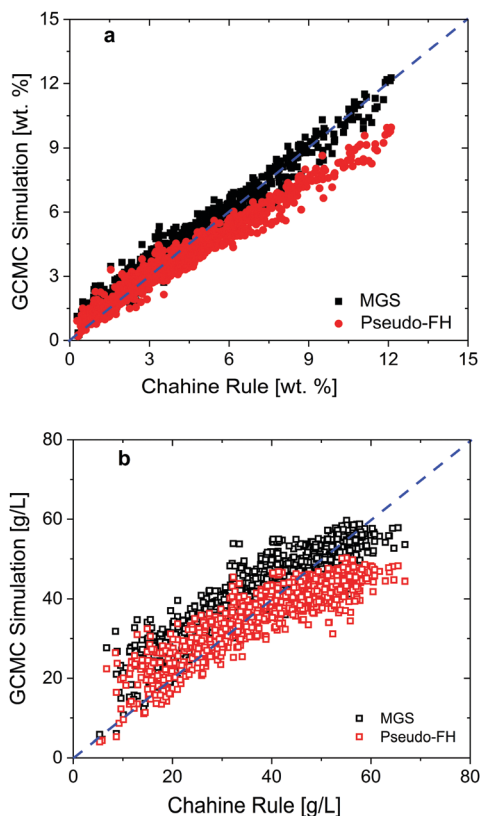


**Fig. 6** Correlation between the Chahine rule and GCMC calculations of total H<sub>2</sub> uptake in approximately 2800 real MOFs with non-zero surface areas. GCMC capacities were calculated at 77 K and 35 bar using both the MGS<sup>80,81</sup> and p-FH<sup>75</sup> potentials for hydrogen. (a) Total gravimetric capacity; (b) total volumetric capacity.

of ~2800 real MOFs (with non-zero porosity) extracted from the UM<sup>27</sup> and CORE<sup>28</sup> databases; comparisons of total volumetric and gravimetric capacity at 77 K and 35 bar are made with both the MGS and p-FH interatomic potentials.

Fig. 6 shows that a strong correlation exists between the Chahine rule and the GCMC-predicted capacities, regardless of the interatomic potential employed. This suggests that relative capacity predictions – *i.e.*, distinguishing MOFs with high (total) capacities from those with low capacities – should be possible with the Chahine rule under these conditions.

The correlation between the methods is strongest for gravimetric capacity, shown in Fig. 6a, especially for the Chahine rule and the MGS-based GCMC simulation. As the MGS potential tends to overestimate measured capacities (Fig. 4 and 5), its strong correlation with the Chahine rule implies that the latter method will yield similar overestimates.

Like the MGS potential, gravimetric predictions from the p-FH-based GCMC exhibit a roughly linear relationship with the Chahine rule. However, the slope of the data trace is shallower. Consequently, at high wt%'s (corresponding to MOFs with high surface areas) the Chahine rule systematically overpredicts capacity relative to the p-FH model. Our observation of overestimation by the Chahine rule is consistent with earlier reports involving high surface area MOFs.<sup>101</sup>

Fig. 6b illustrates the correlation in volumetric H<sub>2</sub> capacity between the Chahine rule and the GCMC-based predictions. While a reasonable correlation still exists, the data exhibit a wider scatter compared to the gravimetric capacity. As observed for the gravimetric data, the Chahine rule is in better agreement with predictions made by the MGS potential. Nevertheless, for the highest capacity MOFs (*i.e.*, those with volumetric capacities exceeding ~60 g H<sub>2</sub> per L) the Chahine rule overpredicts capacity relative to this potential. The overprediction of the Chahine rule is even more severe when compared to the p-FH potential, and is evident for MOFs with capacities exceeding ~45 g H<sub>2</sub> per L. A comparison of Chahine rule and GCMC capacities for a set of high-capacity MOFs reported by Goldsmith *et al.*<sup>27</sup> is given in Table S3 (ESI<sup>†</sup>). Fig. S11 (ESI<sup>†</sup>) illustrates the correlation between total capacity predictions made with the MGS and p-FH-based potentials.

More quantitative measures of the correlation between the Chahine rule and GCMC calculations can be found in Table S4 (ESI<sup>†</sup>), which reports the Pearson correlation coefficient,  $r$ , and the Kendall rank correlation coefficient,  $\tau$ .<sup>102,103</sup> The Pearson coefficient is defined within  $[1, -1]$  and is a measure of the linear correlation between two datasets:  $r = 1(-1)$  implies a perfect positive (negative) correlation. In the present context, a large positive value of  $r$  would indicate, for example, that MOFs predicted to have high capacities according to the Chahine rule also have high capacities based on MGS-based GCMC calculations. In contrast, Kendall's  $\tau$  coefficient assesses the similarity of the pairwise ranking in MOF capacities predicted by two methods (*e.g.*, Chahine rule *vs.* p-FH-based GCMC).  $\tau$  is defined in  $[1, -1]$ , with a value of 1 indicating identical pairwise rank-ordering between the two datasets.

Table S4 (ESI<sup>†</sup>) shows that the Pearson correlation is very high between the Chahine rule and GCMC, regardless of interatomic potential:  $r = 0.98$  for gravimetric capacity, and  $r \sim 0.90$  for volumetric capacity. Moderately lower values are obtained for  $\tau - \sim 0.88$  gravimetric and 0.73 volumetric – indicating that the Chahine rule and GCMC often, but not always, yield the same rank-ordering of MOFs with respect to H<sub>2</sub> capacity. An example of these deviations are shown in Table S3 (ESI<sup>†</sup>), where the Chahine rule predicts EPOTAF to have the highest volumetric capacity, whereas p-FH and MGS-based GCMC predict SUKYN and ENITAX to be the top-performers, respectively.

### High-throughput screening

Fig. 7a illustrates the total volumetric capacities as function of the corresponding gravimetric capacities for 5309 MOFs extracted from the UM<sup>27</sup> and CoRE<sup>28</sup> databases. All calculations were performed at 77 K and 35 bar using the p-FH potential. The rectangular region in the upper right corner identifies 48 compounds that surpass the measured total uptake of MOF-5 (6.8 wt% 44.4 g H<sub>2</sub> per L) at 77 K and 35 bar on both a gravimetric and volumetric basis. A list of these MOFs is given in Table S5 (ESI<sup>†</sup>). In total, only 0.9% of the MOFs examined are predicted to surpass the total capacity of MOF-5. These statistics highlight the



exceptional performance of this well-known compound. Of course, due to pore collapse and stability issues, not all of the compounds identified are likely to achieve the projected performance experimentally.

The concave downward profile of the data in Fig. 7a is similar to what was reported by Goldsmith *et al.*<sup>27</sup> using capacities estimated with the Chahine rule. This shape suggests a tradeoff in volumetric capacity in MOFs that exhibit the highest gravimetric performance.<sup>27</sup> Although several MOFs exhibit impressive gravimetric capacities (exceeding 10 wt%), the data suggest that total volumetric performance is capped at approximately 50 g H<sub>2</sub> per L at 77 K and 35 bar.

Qualitatively different behavior is observed for usable capacities. Fig. 7b plots the usable volumetric vs. usable gravimetric capacity for the same database of MOFs as in Fig. 7a, assuming an isothermal ( $T = 77$  K) pressure swing between 100 and 5 bar. Unlike the concave-downward shape observed for the total capacities (Fig. 7a), the usable volumetric capacity increases monotonically with increasing gravimetric capacity, until a plateau is reached for values  $\geq 8$  wt%. At this point volumetric capacity is capped at a ceiling of  $\sim 40$  g H<sub>2</sub> per L; nevertheless, additional gains in gravimetric capacity are possible, and extend beyond 10 wt%.

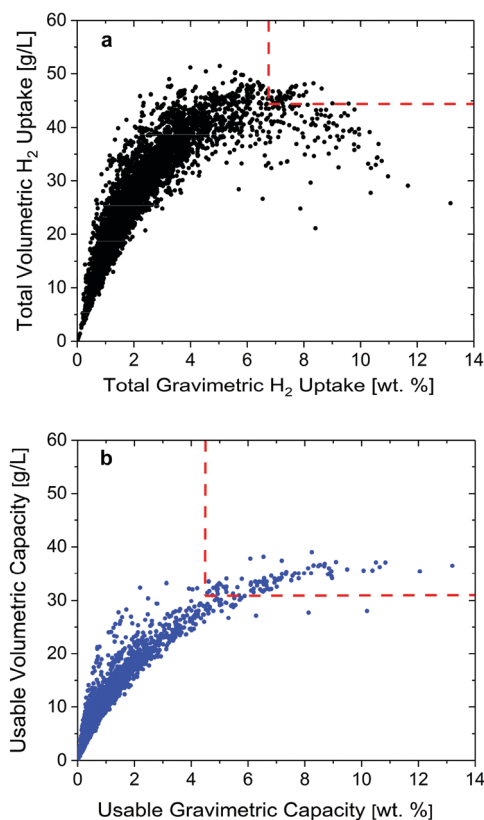


Fig. 7 (a) Total and (b) usable volumetric vs. gravimetric H<sub>2</sub> storage capacities for 5309 MOFs computed at 77 K using GCMC. Total capacities are computed at 35 bar; usable capacities are computed for a pressure swing between 5 and 100 bar. The intersection of the red dashed lines indicates the measured capacity of MOF-5. MOFs that fall to right/above of this point exceed the capacity of MOF-5.

A total of 90 MOFs exceed the usable capacity of MOF-5 (4.5 wt% & 31.1 g L<sup>-1</sup>) both gravimetrically and volumetrically. These compounds, and their respective properties, are listed in Table S6 (ESI<sup>†</sup>). The projected capacities of these MOFs suggest that dramatic gains in (usable) gravimetric capacities, up to 200% higher than MOF-5, may be possible. In contrast, volumetric gains are projected to be much more difficult to achieve, with maximum improvements on the order of only  $\sim 30\%$  compared to MOF-5.

Taken together, these capacity projections (Fig. 7a and b) reaffirm the observation<sup>27</sup> that MOF-5 exhibits a uncommon balance of volumetric and gravimetric performance. Importantly, the volumetric performance of MOF-5 is amongst the best can be achieved within the realm of known MOFs.

### Demonstration of IRMOF-20

Guided by our screening calculations, we aimed to experimentally demonstrate a MOF that can out-perform MOF-5 on a usable capacity basis, both gravimetrically and volumetrically. An assessment of the crystal structures of the highest-capacity compounds (Table S6, ESI<sup>†</sup>) suggested that IRMOF-20 would be a promising target, given prior experience with its synthesis and low (assumed) probability for pore collapse or solvent retention.<sup>104</sup> The structure of IRMOF-20 is shown in Fig. 2. It is isorecticular with MOF-5, and shares the same Zn-based secondary building units (SBUs). Different from MOF-5, the IRMOF-20 linker contains S heteroatoms, and is synthesized using thieno[3,2-*b*]thiophene-2,5-dicarboxylic acid as the precursor.<sup>104</sup>

The calculated hydrogen capacity of IRMOF-20 is summarized in Table 3. Assuming isothermal pressure swing operation between 100 and 5 bar, capacities of 6.1 wt% and 35.5 g H<sub>2</sub> per L were predicted. These values are 36 and 14% higher than the respective capacities of MOF-5.

IRMOF-20 was synthesized and activated according to Rowsell *et al.*<sup>104</sup> Fig. S12 (ESI<sup>†</sup>) shows that the powder XRD pattern of the synthesized material is similar to the simulated pattern generated from the structure from ref. 104. In addition, the measured BET surface area of 4073 m<sup>2</sup> g<sup>-1</sup> was in excellent agreement with the calculated value of 4127 m<sup>2</sup> g<sup>-1</sup>. (The corresponding measured N<sub>2</sub> isotherm is shown in Fig. S13, ESI<sup>†</sup>)

Fig. 8 compares the measured and simulated (total) gravimetric and volumetric H<sub>2</sub> adsorption isotherms for IRMOF-20 at 77 K. Good agreement between theory and experiment was obtained at 77 K and 100 bar: 9.3 (measured) vs. 9.6 (calculated)

Table 3 Usable H<sub>2</sub> storage capacities for IRMOF-20 for an isothermal pressure swing at 77 K between  $P_{\min} = 5$  bar and several maximum pressures,  $P_{\max}$ . MUE is the mean unsigned error between the measurements and calculations

$P_{\max}$ (bar)	Usable grav. (wt%)		Usable vol. (g H <sub>2</sub> per L)	
	Measured	Calculated	Measured	Calculated
35	3.9	4.3	22.3	24.5
50	4.6	5.0	26.3	28.7
100	5.7	6.1	33.4	35.5
MUE		0.40		2.2

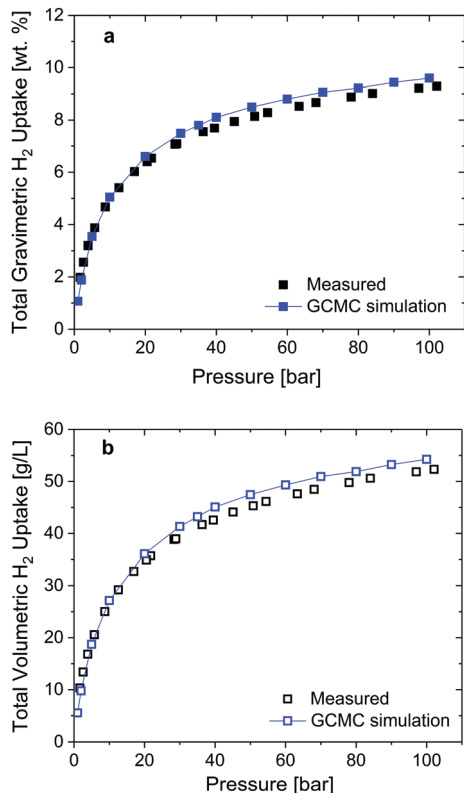


Fig. 8 Measured and calculated total (a) gravimetric and (b) volumetric hydrogen adsorption isotherms of IRMOF-20 at 77 K.

wt% and 52.7 (measured) vs. 54.2 (calculated) g H<sub>2</sub> per L. Based on the total uptake isotherms, Table 3 compares the measured usable pressure-swing capacities of IRMOF-20 with the computationally-predicted values. The measured usable volumetric (33.4 g H<sub>2</sub> per L) and gravimetric (5.7 wt%) capacities of IRMOF-20 for  $P_{\max} = 100$  bar exceed those of MOF-5 (31.1 g H<sub>2</sub> per L & 4.5 wt%, respectively, Table 2) by 7.4% and 26.7%, respectively.

The enhanced gravimetric performance of IRMOF-20 relative to MOF-5 is expected, given its higher surface area:  $\sim 4100$  vs.  $\sim 3500$  m<sup>2</sup> g<sup>-1</sup>, as shown in Table 1. As both compounds share the same SBUs, this extra surface area must be derived from the slightly longer, thiophene-based linkers present in IRMOF-20. On the other hand, the improved volumetric performance of IRMOF-20 (usable basis) does not follow expected trends related to total volumetric capacity. For example, the density and volumetric surface area (VSA) of MOF-5 are both larger than those of IRMOF-20: 0.60 vs. 0.51 g cm<sup>-3</sup> and 2172 vs. 2000 m<sup>2</sup> cm<sup>-3</sup>, respectively. As expected, these properties correlate positively with the higher total volumetric hydrogen capacity exhibited by MOF-5, yet these same properties correlate negatively with usable volumetric capacity. Furthermore, void fraction and pore volume – two properties expected to correlate with gravimetric density – appear to correlate positively with usable volumetric capacity (Table 1). Additional study is needed to clarify trends linking usable volumetric capacity and fundamental structural properties of MOFs.

Table 4 Measured usable capacities of selected MOFs assuming a temperature + pressure swing from ( $T_{\min} = 77$  K,  $P_{\max} = 100$  bar) to ( $T_{\max} = 160$  K,  $P_{\min} = 5$  bar)

MOF	Usable gravimetric H <sub>2</sub> capacity (wt%)	Usable volumetric H <sub>2</sub> capacity (g H <sub>2</sub> per L)
MOF-5	7.8	51.9
IRMOF-20	9.1	51.0
NU-1103	12.6	43.2

### IRMOF-20 compared to other high-capacity MOFs

To place the properties of IRMOF-20 in context, it is helpful to compare its performance to other recently-reported high-capacity MOFs. For example, Gómez-Gualdrón *et al.*<sup>4</sup> reported usable gravimetric and volumetric capacities of NU-1103 assuming a temperature + pressure swing from ( $T_{\min} = 77$  K,  $P_{\max} = 100$  bar) to ( $T_{\max} = 160$  K,  $P_{\min} = 5$  bar). Table 4 compares the performance of MOF-5, IRMOF-20, and NU-1103 using these operating conditions. The data illustrate the superior volumetric performance of MOF-5 and IRMOF-20: both of these MOFs exhibit usable capacities of approximately 51 g H<sub>2</sub> per L, a value  $\sim 20\%$  larger than that for NU-1103. On the other hand, NU-1103 excels gravimetrically, outperforming both MOF-5 and IRMOF-20 by 61% and 38%, respectively.

Overall, the performance of IRMOF-20 exhibits an appealing balance, as it achieves high usable gravimetric and volumetric capacities simultaneously. MOFs with balanced, high capacities are rare (for example, see Fig. 7). The ability of IRMOF-20 to out-perform the usable capacity of MOF-5 suggests that it can serve as a new benchmark against which future storage materials can be assessed. As a known MOF that was first reported more than a decade ago,<sup>104</sup> the identification of IRMOF-20 highlights the value of computational screening in identifying existing, but overlooked materials. We anticipate that additional MOF ‘diamonds in the rough’ will be identified using this approach.<sup>4,9,21,28,38,105–108</sup>

In a broader sense, the variations in performance observed between IRMOF-20 and MOF-5 for the different operating conditions examined (*e.g.*, isothermal pressure swing vs. temperature + pressure swing) highlight the impact of these conditions on usable capacity. Fortunately, the methods employed here could be exploited to identify the best MOF for a fixed operating scenario, or conversely, to quantify the gains in capacity that could be achieved with other scenarios. Of course, in the latter case a gain in capacity should be weighed against penalties that could be incurred at the system level, such as efficiency losses arising from more significant heating/cooling loads.<sup>45,46,48,64</sup>

## Conclusions

Metal organic frameworks (MOFs) are promising hydrogen storage materials thanks to their high surface areas, tunable properties, and reversible gas adsorption. Although several MOFs are known to exhibit high hydrogen densities on a gravimetric basis, realizing high volumetric capacities remains a challenge. The present study demonstrates MOFs capable of

achieving high gravimetric and volumetric H<sub>2</sub> densities simultaneously using a combination of computational screening, synthesis, and characterization.

The hydrogen capacities of 5309 MOFs drawn from databases of known compounds were predicted using empirical correlations and grand canonical Monte Carlo simulations. Correlations between these two methods, and with experimental data, were quantified. These assessments identified pseudo-Feynman–Hibbs-based GCMC calculations as the method yielding the best agreement with measured capacities. Nevertheless, the relatively strong correlation observed between the Chahine rule and more expensive GCMC calculations suggests that the former method remains a useful tool for quickly assessing the H<sub>2</sub> capacity of MOFs.

Promising MOFs suggested by screening were synthesized and evaluated with respect to their usable H<sub>2</sub> capacities. Unfortunately, several MOFs predicted to exhibit high capacities were unstable upon activation, highlighting the need to understand the factors that contribute to pore collapse. Consistent with the computational predictions, IRMOF-20 was experimentally demonstrated to exhibit high usable volumetric and gravimetric capacities. These capacities exceed those of the benchmark compound MOF-5, and establish a new high-water mark for usable hydrogen capacity in MOFs. Our study illustrates the value of computational screening in guiding experimental efforts towards materials that optimize overall storage performance.

## Conflicts of interest

There are no conflicts to declare.

## Acknowledgements

Financial support for this study was provided by the US Department of Energy, Office of Energy Efficiency and Renewable Energy, Grant no. DE-EE0007046. Partial computing resources were provided by the NSF *via* grant 1531752 MRI: Acquisition of Conflux, A Novel Platform for Data-Driven Computational Physics (Tech. Monitor: Ed Walker).

## References

- J. Yang, A. Sudik, C. Wolverton and D. J. Siegel, *Chem. Soc. Rev.*, 2010, **39**, 656–675.
- N. L. Rosi, J. Eckert, M. Eddaoudi, D. T. Vodak, J. Kim, M. O’Keeffe and O. M. Yaghi, *Science*, 2003, **300**, 1127–1129.
- J. L. C. Rowsell and O. M. Yaghi, *Angew. Chem., Int. Ed.*, 2005, **44**, 4670–4679.
- D. A. Gómez-Gualdrón, Y. J. Colón, X. Zhang, T. C. Wang, Y.-S. Chen, J. T. Hupp, T. Yildirim, O. K. Farha, J. Zhang and R. Q. Snurr, *Energy Environ. Sci.*, 2016, **9**, 3279–3289.
- Y. Sun, L. Wang, W. A. Amer, H. Yu, J. Ji, L. Huang, J. Shan and R. Tong, *J. Inorg. Organomet. Polym. Mater.*, 2013, **23**, 270–285.
- J. R. Long, *Hydrogen Storage in Metal-Organic Frameworks*, U.S. Department of Energy, Hydrogen and Fuel Cells Program 2015 Annual Merit Review Proceedings, Project ST103, [https://www.hydrogen.energy.gov/pdfs/review15/st103\\_long\\_2015\\_o.pdf](https://www.hydrogen.energy.gov/pdfs/review15/st103_long_2015_o.pdf).
- D. Gygi, E. D. Bloch, J. A. Mason, M. R. Hudson, M. I. Gonzalez, R. L. Siegelman, T. A. Darwish, W. L. Queen, C. M. Brown and J. R. Long, *Chem. Mater.*, 2016, **28**, 1128–1138.
- D. J. Collins and H.-C. Zhou, *J. Mater. Chem.*, 2007, **17**, 3154–3160.
- M. P. Suh, H. J. Park, T. K. Prasad and D.-W. Lim, *Chem. Rev.*, 2012, **112**, 782–835.
- O. M. Yaghi and H. Li, *J. Am. Chem. Soc.*, 1995, **117**, 10401–10402.
- H.-C. ‘Joe’ Zhou and S. Kitagawa, *Chem. Soc. Rev.*, 2014, **43**, 5415–5418.
- H.-C. Zhou, J. R. Long and O. M. Yaghi, *Chem. Rev.*, 2012, **112**, 673–674.
- S. R. Batten, N. R. Champness, X.-M. Chen, J. Garcia-Martinez, S. Kitagawa, L. Öhrström, M. O’Keeffe, M. Paik Suh and J. Reedijk, *Pure Appl. Chem.*, 2013, **85**, 1715–1724.
- S. R. Batten, N. R. Champness, X.-M. Chen, J. Garcia-Martinez, S. Kitagawa, L. Öhrström, M. O’Keeffe, M. P. Suh and J. Reedijk, *CrystEngComm*, 2012, **14**, 3001.
- L. Öhrström, *Crystals*, 2015, **5**, 154–162.
- R. A. Fischer and I. Schwedler, *Angew. Chem.*, 2014, **126**, 7209–7214.
- A. J. Howarth, A. W. Peters, N. A. Vermeulen, T. C. Wang, J. T. Hupp and O. K. Farha, *Chem. Mater.*, 2017, **29**, 26–39.
- D. A. Gómez-Gualdrón, P. Z. Moghadam, J. T. Hupp, O. K. Farha and R. Q. Snurr, *J. Am. Chem. Soc.*, 2016, **138**, 215–224.
- T. F. Willems, C. H. Rycroft, M. Kazi, J. C. Meza and M. Haranczyk, *Microporous Mesoporous Mater.*, 2012, **149**, 134–141.
- M. Pinheiro, R. L. Martin, C. H. Rycroft, A. Jones, E. Iglesia and M. Haranczyk, *J. Mol. Graphics Modell.*, 2013, **44**, 208–219.
- R. L. Martin, B. Smit and M. Haranczyk, *J. Chem. Inf. Model.*, 2012, **52**, 308–318.
- K. S. Walton and R. Q. Snurr, *J. Am. Chem. Soc.*, 2007, **129**, 8552–8556.
- K. K. Gangu, S. Maddila, S. B. Mukkamala and S. B. Jonnalagadda, *Inorg. Chim. Acta*, 2016, **446**, 61–74.
- M. S. Denny, J. C. Moreton, L. Benz and S. M. Cohen, *Nat. Rev. Mater.*, 2016, **1**, 1–17.
- Y. J. Colón and R. Q. Snurr, *Chem. Soc. Rev.*, 2014, **43**, 5735–5749.
- S. Furukawa, J. Reboul, S. Diring, K. Sumida and S. Kitagawa, *Chem. Soc. Rev.*, 2014, **43**, 5700–5734.
- J. Goldsmith, A. G. Wong-Foy, M. J. Cafarella and D. J. Siegel, *Chem. Mater.*, 2013, **25**, 3373–3382.
- Y. G. Chung, J. Camp, M. Haranczyk, B. J. Sikora, W. Bury, V. Krungleviciute, T. Yildirim, O. K. Farha, D. S. Sholl and R. Q. Snurr, *Chem. Mater.*, 2014, **26**, 6185–6192.
- P. Z. Moghadam, A. Li, S. B. Wiggin, A. Tao, A. G. P. Maloney, P. A. Wood, S. C. Ward and D. Fairen-Jimenez, *Chem. Mater.*, 2017, **29**, 2618–2625.

- 30 C. E. Wilmer, M. Leaf, C. Y. Lee, O. K. Farha, B. G. Hauser, J. T. Hupp and R. Q. Snurr, *Nat. Chem.*, 2011, **4**, 83–89.
- 31 D. A. Gómez-Gualdrón, P. Z. Moghadam, J. T. Hupp, O. K. Farha and R. Q. Snurr, *J. Am. Chem. Soc.*, 2016, **138**, 215–224.
- 32 H. Frost, T. Düren and R. Q. Snurr, *J. Phys. Chem. B*, 2006, **110**, 9565–9570.
- 33 Y.-S. Bae and R. Q. Snurr, *Microporous Mesoporous Mater.*, 2010, **132**, 300–303.
- 34 M. A. Addicoat, D. E. Coupry and T. Heine, *J. Phys. Chem. A*, 2014, **118**, 9607–9614.
- 35 P. G. Boyd and T. K. Woo, *CrystEngComm*, 2016, **18**, 3777–3792.
- 36 D. J. Tranchemontagne, J. L. Mendoza-Cortés, M. O’Keeffe and O. M. Yaghi, *Chem. Soc. Rev.*, 2009, **38**, 1257.
- 37 T. Düren, Y.-S. Bae and R. Q. Snurr, *Chem. Soc. Rev.*, 2009, **38**, 1237.
- 38 C. M. Simon, J. Kim, D. A. Gómez-Gualdrón, J. S. Camp, Y. G. Chung, R. L. Martin, R. Mercado, M. W. Deem, D. Gunter, M. Haranczyk, D. S. Sholl, R. Q. Snurr and B. Smit, *Energy Environ. Sci.*, 2015, **8**, 1190–1199.
- 39 N. S. Bobbitt, J. Chen and R. Q. Snurr, *J. Phys. Chem. C*, 2016, **120**, 27328–27341.
- 40 C. R. Groom, I. J. Bruno, M. P. Lightfoot and S. C. Ward, *Acta Cryst.*, 2016, **72**, 171–179.
- 41 B. Panella, M. Hirscher and S. Roth, *Carbon*, 2005, **43**, 2209–2214.
- 42 M. Kondo, Y. Irie, M. Miyazawa, H. Kawaguchi, S. Yasue, K. Maeda and F. Uchida, *J. Organomet. Chem.*, 2007, **692**, 136–141.
- 43 T. K. Kim and M. P. Suh, *Chem. Commun.*, 2011, **47**, 4258–4260.
- 44 L. Ma, A. Jin, Z. Xie and W. Lin, *Angew. Chem., Int. Ed.*, 2009, **48**, 9905–9908.
- 45 M. Veenstra, J. Yang, C. Xu, M. Gaab, L. Arnold, U. Muller, D. J. Siegel and Y. Ming, Ford/BASF-SE/UM Activities in Support of the Hydrogen Storage Engineering Center of Excellence, U.S. Department of Energy, Hydrogen and Fuel Cells Program 2014 Annual Merit Review Proceedings: Project ST010, [https://www.hydrogen.energy.gov/pdfs/review14/st010\\_veenstra\\_2014\\_o.pdf](https://www.hydrogen.energy.gov/pdfs/review14/st010_veenstra_2014_o.pdf).
- 46 DOE Technical Targets for Onboard Hydrogen Storage for Light-Duty Vehicles, <https://energy.gov/eere/fuelcells/doe-Technical-Targets-Onboard-Hydrogen-Storage-Light-Duty-Vehicles>.
- 47 J. A. Mason, M. Veenstra and J. R. Long, *Chem. Sci.*, 2014, **5**, 32–51.
- 48 D. L. Anton and T. Motyka, Hydrogen Storage Engineering Center of Excellence, U.S. Department of Energy, Hydrogen and Fuel Cells Program 2015 Annual Merit Review Proceedings, Project ST004, [https://www.hydrogen.energy.gov/pdfs/review15/st004\\_anton\\_2015\\_o.pdf](https://www.hydrogen.energy.gov/pdfs/review15/st004_anton_2015_o.pdf).
- 49 J. Purewal, D. Liu, A. Sudik, M. Veenstra, J. Yang, S. Maurer, U. Müller and D. J. Siegel, *J. Phys. Chem. C*, 2012, **116**, 20199–20212.
- 50 D. P. Broom, C. J. Webb, K. E. Hurst, P. A. Parilla, T. Gennett, C. M. Brown, R. Zacharia, E. Tylanakis, E. Klontzas, G. E. Froudakis, T. A. Steriotis, P. N. Trikalitis, D. L. Anton, B. Hardy, D. Tamburello, C. Corgnale, B. A. van Hassel, D. Cossement, R. Chahine and M. Hirscher, *Appl. Phys. A: Mater. Sci. Process.*, 2016, **122**, 151.
- 51 R. B. Getman, Y.-S. Bae, C. E. Wilmer and R. Q. Snurr, *Chem. Rev.*, 2012, **112**, 703–723.
- 52 M. Wahiduzzaman, C. F. J. Walther and T. Heine, *J. Chem. Phys.*, 2014, **141**, 64708.
- 53 Y. Basdogan and S. Keskin, *CrystEngComm*, 2015, **17**, 261–275.
- 54 D. Durette, P. Bénard, R. Zacharia and R. Chahine, *Sci. Bull.*, 2016, **61**, 594–600.
- 55 R. J. Sadus, *Molecular simulation of fluids: theory, algorithms, and object-orientation*, Elsevier, Amsterdam, 1999.
- 56 T. L. Hill, *An introduction to statistical thermodynamics*, Dover Publications, 1986.
- 57 A. K. Rappe, C. J. Casewit, K. S. Colwell, W. A. Goddard and W. M. Skiff, *J. Am. Chem. Soc.*, 1992, **114**, 10024–10035.
- 58 M. A. Addicoat, N. Vankova, I. F. Akter and T. Heine, *J. Chem. Theory Comput.*, 2014, **10**, 880–891.
- 59 D. E. Coupry, M. A. Addicoat and T. Heine, *J. Chem. Theory Comput.*, 2016, **12**, 5215–5225.
- 60 H. Furukawa, M. A. Miller and O. M. Yaghi, *J. Mater. Chem.*, 2007, **17**, 3197.
- 61 R. P. Feynman and A. R. Hibbs, *Quantum mechanics and path integrals*, McGraw-Hill, New York, 1965.
- 62 A. Kuc, T. Heine, G. Seifert and H. A. Duarte, *Theor. Chem. Acc.*, 2008, **120**, 543–550.
- 63 J. Liu, J. T. Culp, S. Natesakhawat, B. C. Bockrath, B. Zande, S. G. Sankar, G. Garberoglio and J. K. Johnson, *J. Phys. Chem. C*, 2007, **111**, 9305–9313.
- 64 D. J. Siegel, B. Hardy and the HSECoE Team, Engineering an Adsorbent-Based Hydrogen Storage System: What Have We Learned?, Hydrogen Storage Summit, Golden, CO – January 27–28, 2015, [https://energy.gov/sites/prod/files/2015/02/f19/fcto\\_h2\\_storage\\_summit\\_siegel.pdf](https://energy.gov/sites/prod/files/2015/02/f19/fcto_h2_storage_summit_siegel.pdf), accessed 9 May 2017.
- 65 S. S. Kaye, A. Dailly, O. M. Yaghi and J. R. Long, *J. Am. Chem. Soc.*, 2007, **129**, 14176–14177.
- 66 A. G. Wong-Foy, A. J. Matzger and O. M. Yaghi, *J. Am. Chem. Soc.*, 2006, **128**, 3494–3495.
- 67 C. H. Rycroft, *Chaos*, 2009, **19**, 41111.
- 68 J. J. Potoff and J. I. Siepmann, *AIChE J.*, 2001, **47**, 1676–1682.
- 69 H. A. Lorentz, *Ann. Phys.*, 1881, **248**, 127–136.
- 70 S. I. Sandler, *Chemical, biochemical, and engineering thermodynamics*, Wiley, 4th edn, 2006.
- 71 O. Talu and A. L. Myers, *AIChE J.*, 2001, **47**, 1160–1168.
- 72 D. Dubbeldam, S. Calero, D. E. Ellis and R. Q. Snurr, *Mol. Simul.*, 2016, **42**, 81–101.
- 73 D. Dubbeldam, A. Torres-Knoop and K. S. Walton, *Mol. Simul.*, 2013, **39**, 14–15.
- 74 M. Hirscher, *Angew. Chem., Int. Ed.*, 2011, **50**, 581–582.
- 75 M. Fischer, F. Hoffmann and M. Fröba, *ChemPhysChem*, 2009, **10**, 2647–2657.
- 76 V. Buch, *J. Chem. Phys.*, 1994, **100**, 7610.



- 77 A. V. A. Kumar, H. Jobic and S. K. Bhatia, *J. Phys. Chem. B*, 2006, **110**, 16666–16671.
- 78 F. Darkrim and D. Levesque, *J. Chem. Phys.*, 1998, **109**, 4981.
- 79 F. Darkrim, A. Aoufi, P. Malbrunot and D. Levesque, *J. Chem. Phys.*, 2000, **112**, 5991.
- 80 A. Michels, W. de Graaff and C. A. Ten Seldam, *Physica*, 1960, **26**, 393–408.
- 81 P. Ryan, L. J. Broadbelt and R. Q. Snurr, *Chem. Commun.*, 2008, 4132.
- 82 D. Frenkel and B. Smit, *Understanding molecular simulation: from algorithms to applications*, Academic Press, Inc., Orlando, FL, 2nd edn, 2001.
- 83 S. I. Sandler, *An Introduction to Applied Statistical Thermodynamics*, John Wiley & Son Ltd, New York, NY, 2010.
- 84 Y. Ming, J. Purewal, A. Liu, A. Sudik, C. Xu, J. Yang, M. Veenstra, K. Rhodes, R. Soltis, J. Warner, M. Gaab, U. Müller and D. J. Siegel, *Microporous Mesoporous Mater.*, 2014, **185**, 235–244.
- 85 J. E. Mondloch, O. Karagiari, O. K. Farha and J. T. Hupp, *CrystEngComm*, 2013, **15**, 9258–9264.
- 86 R. Grünker, V. Bon, P. Mü, U. Stoeck, S. Krause, U. Mueller, I. Senkovska and S. Kaskel, *Chem. Commun.*, 2014, **50**, 3450.
- 87 B. Liu, A. G. Wong-Foy and A. J. Matzger, *Chem. Commun.*, 2013, **49**, 1419.
- 88 M. Thommes, K. Kaneko, A. V. Neimark, J. P. Olivier, F. Rodriguez-Reinoso, J. Rouquerol and K. S. W. Sing, *Pure Appl. Chem.*, 2015, **87**, 1051–1069.
- 89 P. A. Parilla, K. Gross, K. Hurst and T. Gennett, *Appl. Phys. A: Mater. Sci. Process.*, 2016, **122**, 201.
- 90 E. Poirier and A. Dailly, *J. Phys. Chem. C*, 2008, **112**, 13047–13052.
- 91 J. Rouquerol, F. Rouquerol and K. Sing, *Adsorption by powders and porous solids: principles, methodology and applications*, Academic Press, San Diego, CA, 1st edn, 1999.
- 92 J. Rouquerol, P. Llewellyn and F. Rouquerol, *Stud. Surf. Sci. Catal.*, 1998, **160**, 49–56.
- 93 D. Yuan, D. Zhao and H.-C. Zhou, *Inorg. Chem.*, 2011, **50**, 10528–10530.
- 94 A. Schneemann, V. Bon, I. Schwedler, I. Senkovska, S. Kaskel and R. A. Fischer, *Chem. Soc. Rev.*, 2014, **43**, 6062–6096.
- 95 M. P. Allen and D. J. Tildesley, *Computer simulation of liquids*, Oxford University Press, New York, NY, 1989.
- 96 M. Fischer, *Molecular Simulations of Hydrogen Storage and Gas Separation in Metal–Organic Frameworks*, PhD dissertation, University of Hamburg, 2011.
- 97 E. Lemmon, M. McLinden and D. Friend, Thermophysical Properties of Fluid System, in *NIST Chemistry WebBook, NIST Standard Reference Database Number 69*, ed. P. J. Linstrom and W. G. Mallard, National Institute of Standards and Technology, Gaithersburg, MD, <http://webbook.nist.gov/chemistry/>.
- 98 K. Koh, A. G. Wong-Foy and A. J. Matzger, *J. Am. Chem. Soc.*, 2010, **132**, 15005–15010.
- 99 A. Dutta, K. Koh, A. G. Wong-Foy and A. J. Matzger, *Angew. Chem., Int. Ed.*, 2015, **54**, 3983–3987.
- 100 N. Klein, I. Senkovska, I. A. Baburin, R. Grünker, U. Stoeck, M. Schlichtenmayer, B. Streppel, U. Mueller, S. Leoni, M. Hirscher and S. Kaskel, *Chem. – Eur. J.*, 2011, **17**, 13007–13016.
- 101 H. Oh, *Nanoporous Materials for Hydrogen Storage and H<sub>2</sub>/D<sub>2</sub> Isotope Separation*, PhD thesis, Max Planck Institute for Intelligent Systems, University of Stuttgart, 2014.
- 102 M. G. Kendall, *Biometrika*, 1938, **30**, 81–93.
- 103 W. H. Press, *Numerical recipes: the art of scientific computing*, Cambridge University Press, 2007.
- 104 J. L. C. Rowsell and O. M. Yaghi, *J. Am. Chem. Soc.*, 2006, **128**, 1304.
- 105 D. A. Gómez-Gualdrón, C. E. Wilmer, O. K. Farha, J. T. Hupp and R. Q. Snurr, *J. Phys. Chem. C*, 2014, **118**, 6941–6951.
- 106 Y. G. Chung, D. A. Gómez-Gualdrón, P. Li, K. T. Leperi, P. Deria, H. Zhang, N. A. Vermeulen, J. F. Stoddart, F. You, J. T. Hupp, O. K. Farha and R. Q. Snurr, *Sci. Adv.*, 2016, **2**, e1600909.
- 107 Y. Bao, R. L. Martin, M. Haranczyk and M. W. Deem, *Phys. Chem. Chem. Phys.*, 2015, **17**, 11962–11973.
- 108 M. Witman, S. Ling, A. Gladysiak, K. C. Stylianou, B. Smit, B. Slater and M. Haranczyk, *J. Phys. Chem. C*, 2017, **121**, 1171–1181.